Cell Stem Cell
Short Article

Generation of Multipotent Induced Neural Crest by Direct Reprogramming of Human Postnatal Fibroblasts with a Single Transcription Factor

Yong Jun Kim,[1,2] Hotae Lim,[1] Zhe Li,[3] Yohan Oh,[1,2] Irina Kovlyagina,[1] In Young Choi,[1] Xinzhong Dong,[3,4,5] and Gabsang Lee[1,2,3,*]
[1]Institute for Cell Engineering, Johns Hopkins University School of Medicine, Baltimore, MD 21205, USA
[2]Department of Neurology, Johns Hopkins University School of Medicine, Baltimore, MD 21205, USA
[3]The Solomon H. Snyder Department of Neuroscience, Johns Hopkins University School of Medicine, Baltimore, MD 21205, USA
[4]Center for Sensory Biology, Johns Hopkins University School of Medicine, Baltimore, MD 21205, USA
[5]The Howard Hughes Medical Institute, Baltimore, MD 21205, USA
*Correspondence: glee48@jhmi.edu
http://dx.doi.org/10.1016/j.stem.2014.07.013

SUMMARY

Neural crest (NC) generates diverse lineages including peripheral neurons, glia, melanocytes, and mesenchymal derivatives. Isolating multipotent human NC has proven challenging, limiting our ability to understand NC development and model NC-associated disorders. Here, we report direct reprogramming of human fibroblasts into induced neural crest (iNC) cells by overexpression of a single transcription factor, SOX10, in combination with environmental cues including WNT activation. iNC cells possess extensive capacity for migration in vivo, and single iNC clones can differentiate into the four main NC lineages. We further identified a cell surface marker for prospective isolation of iNCs, which was used to generate and purify iNCs from familial dysautonomia (FD) patient fibroblasts. FD-iNC cells displayed defects in cellular migration and alternative mRNA splicing, providing insights into FD pathogenesis. Thus, this study provides an accessible platform for studying NC biology and disease through rapid and efficient reprogramming of human postnatal fibroblasts.

INTRODUCTION

During development, various cellular fates in our body are determined by intercellular signaling cascades and cell-type-specific gene expression patterns. These cell determination processes are often elicited by cell extrinsic factors, such as growth factors, morphogens, and extracellular matrix, released from neighboring cells in a spatiotemporally controlled manner. Recent studies have shown that particular combinations of transcription factors can force human somatic cells into new identities, including pluripotent stem cells (Park et al., 2008; Takahashi and Yamanaka, 2006), postmitotic neurons (Pang et al., 2011), myoblasts (Schäfer et al., 1990), etc. Such genetic factors may be replaced by environmental elements or cell extrinsic cues for certain cell types; for example, the formation, proliferation, and differentiation of neural crest (NC) cells are contingent upon and triggered by the interaction of several signaling pathways (Sieber-Blum and Zhang, 1997), including WNT, BMP, and FGF molecules provided by adjacent tissues, such as neural plate, epidermis, mesodermal cells, etc. Therefore, the direct conversion of human somatic cells into the NC fate might be attained by environmental cues with minimal genetic intervention. Here, we set out to determine whether different cell extrinsic factors together with a single transcription factor are sufficient to convert normal human fibroblasts directly into induced NC (iNC), demonstrating the feasibility of further isolation of disease-specific iNCs directly from patient fibroblasts.

RESULTS

To identify the factors sufficient for iNC generation from fibroblasts, we used a *Sox10::eGFP* reporter human embryonic stem cell (hESC) line (Lee et al., 2010), because SOX10 is one of the most characterized NC genetic markers (Betancur et al., 2010; Kelsh, 2006). This genetic reporter hESC line faithfully expresses eGFP for *SOX10* expression in NC differentiation (Figures S1A–S1D, available online). To confirm that the fibroblasts are not in any "partial stem-like" or "intermediate differentiation" stages, we confirmed that their fibroblasts do not have any eGFP expression, pluripotent stem cell marker or *SOX10* expression, and further methylation status of *NANOG* (Figures S1E–S1J) before performing qRT-PCR for *NESTIN* ($<10^5$ compared to hESC-derived neural progenitors) and antibody staining for NESTIN (0 out of 1,535 cells), PAX3 (0 out of 1,516 cells), PAX6 (0 out of 1,672 cells), and PAX7 (0 out of 1,483 cells) (data not shown). Because SOX10 is a key transcription factor for the NC lineage (Betancur et al., 2010), we hypothesized that SOX10 could be one of the minimal genetic factors for iNC induction. For a "tunable" SOX10 overexpression system, doxycycline (DOX)-inducible lentiviruses containing *SOX10* cDNA were infected into the *Sox10::eGFP* fibroblasts (termed *Sox10::eGFP* fibroblasts) (Figure 1A). After screening of various conditions, we found that a combination of SOX10 overexpression

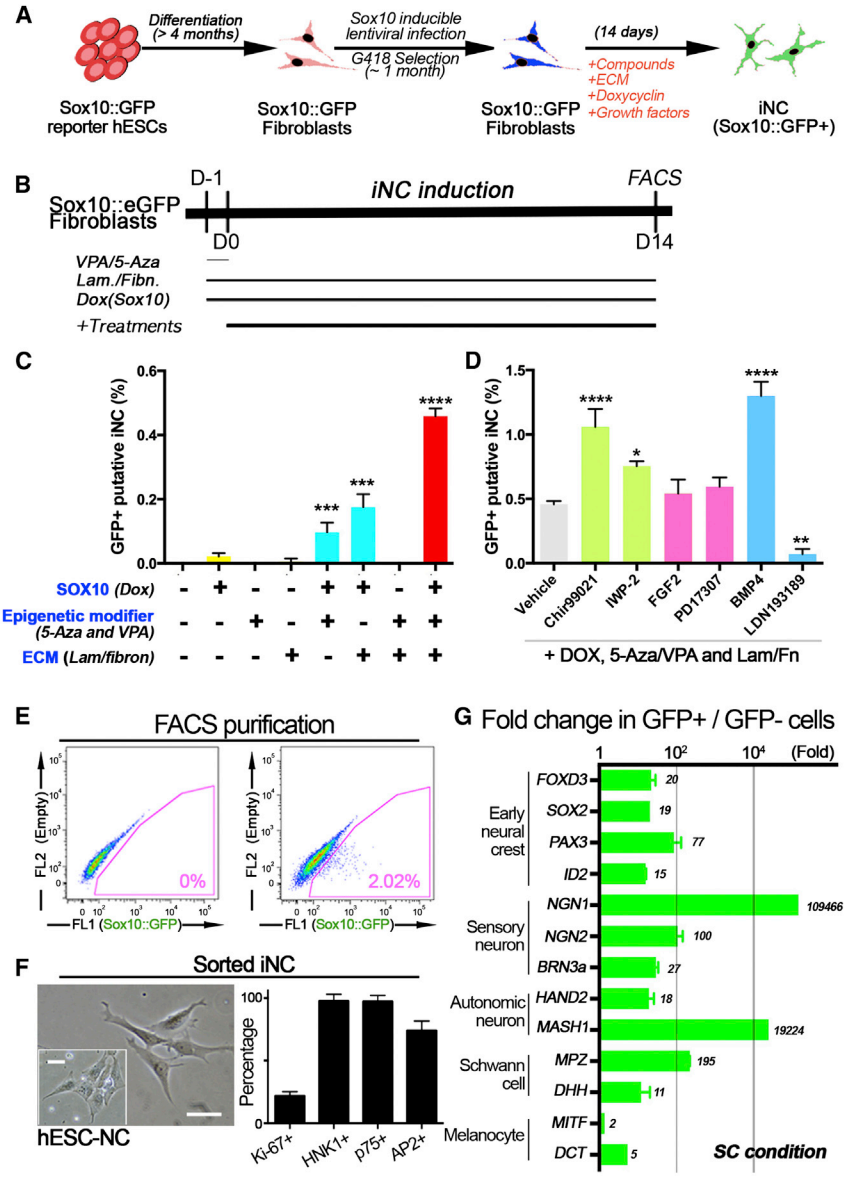

Figure 1. Cell Extrinsic Factors Can Induce eGFP Expression in *Sox10::eGFP* Reporter Fibroblasts

(A) Scheme of induced neural crest (iNC) derivation.

(B) Treatment duration of SOX10 overexpression (Dox), extracellular matrix (ECM), and epigenetic modifiers (epiM).

(C) Combined treatment of Dox, ECM, and epiM can substantially induce eGFP expression in *Sox10::eGFP* reporter fibroblasts.

(D) Chir99021 or BMP4 treatment during iNC induction can significantly enhance the number of eGFP-expressing cells.

(E) Representative FACS plot of *Sox10::eGFP* reporter fibroblasts after iNC induction (Day 14).

(F) FACS-purified eGFP-expressing iNCs and hESC-NCs (inset panel) share characteristic morphology and show immunoreactivity to Ki-67, AP2, p75, and HNK1 antibodies.

(G) Expression levels of NC marker genes between eGFP+ and eGFP− populations assessed by qRT-PCR analysis. *$p < 0.05$; **$p < 0.01$; ****$p < 0.0001$. All scale bars correspond to 50 μm. n = 3–8. All values are mean and SD. See also Figure S1.

and extracellular matrix components such as fibronectin/laminin (FN/Lam) and epigenetic modifiers and 5-Aza-2′-deoxycytidine/Valproic acid (5-Aza/VPA) yields consistent eGFP expression (0.45% ± 0.01%) (Figures 1B–1C and Figures S1K and S1L), a comparable efficacy to that of other cell types (Sekiya and Suzuki, 2011; Son et al., 2011; Vierbuchen et al., 2010).

Neural crest fate is modulated by extrinsic patterning factors, as shown in mammalian development (Sieber-Blum, 2000) as well as hESC studies (Lee et al., 2007). After DOX (SOX10), FN/Lam, and 5-Aza/VPA treatment, we observed a significant increase in eGFP+ cells upon exposure to WNT (Chir99021, 1.06% ± 0.08%, $p < 0.0001$; WNT3a, 0.56% ± 0.02%, $p < 0.05$) and BMP4 (1.3% ± 0.06%, $p < 0.0001$) activation (Figure 1D and Figures S1M and S1N), while antagonists of WNT (IWP-2) and BMP (LDN193189) inhibited induction of eGFP+ cells, which were confirmed with multiple combination treatment experiments (Figure S1O). In a time course analysis (Figure S1P), the eGFP induction level with either Chir99021 or BMP4 in the presence of SOX10/FN/Lam/5Aza/VPA is comparable.

Isolated eGFP-expressing cells (Figure 1E) have morphological similarity with hESC-derived NC cells (hESC-NC cells) (Figure 1F and Figure S1Q), express Ki-67, HNK1, p75, and AP2 protein (21.75% ± 3.49%, 97.5% ± 5.59%, 73.8 ± 7.85%, and 97.2% ± 4.81%, respectively) 24 hr after cell sorting (Figure 1F and Figure S1R), and could maintain SOX10 expression (73.7% ± 15.65%) even after 1 week of culture without DOX treatment (Figures S1S and S1T). Interestingly, the Sox10::eGFP+ cells under WNT activation, but not those under BMP activation (Figure S1U), showed increased levels of NC marker gene expression (Figure 1G). Antibody staining for pSMAD1/5 shows that Sox10::eGFP fibroblasts (grown in 10% FBS) have enough BMP activation level that is abolished by TGF-beta inhibitors (LDN193189 and SB431542) (Figures S1V and S1W). Furthermore, our iNC population can be propagated in culture with multiple passages (at least 4 weeks) (Figure S1X), demonstrating that isolated iNCs could survive without losing proliferation ability and NC identity even after SOX10 withdrawal (Figures 1F–1G and Figures S1S, S1T, and S1X). In addition, using an *OCT4::eGFP* reporter system, we confirmed that our iNC protocol does not contain any detectable pluripotent intermediate stage (Figure S1Y).

Next, we examined the fact that NC marker gene expression in eGFP+ iNCs was significantly upregulated (*p75*, $p < 0.0001$; endogenous *SOX10*, $p < 0.0001$; *FOXD3*, $p < 0.0001$) (Figure 2A and Figure S2A), compared to the uninduced population (*Sox10::eGFP* fibroblasts). Meanwhile, oligodendrocyte markers

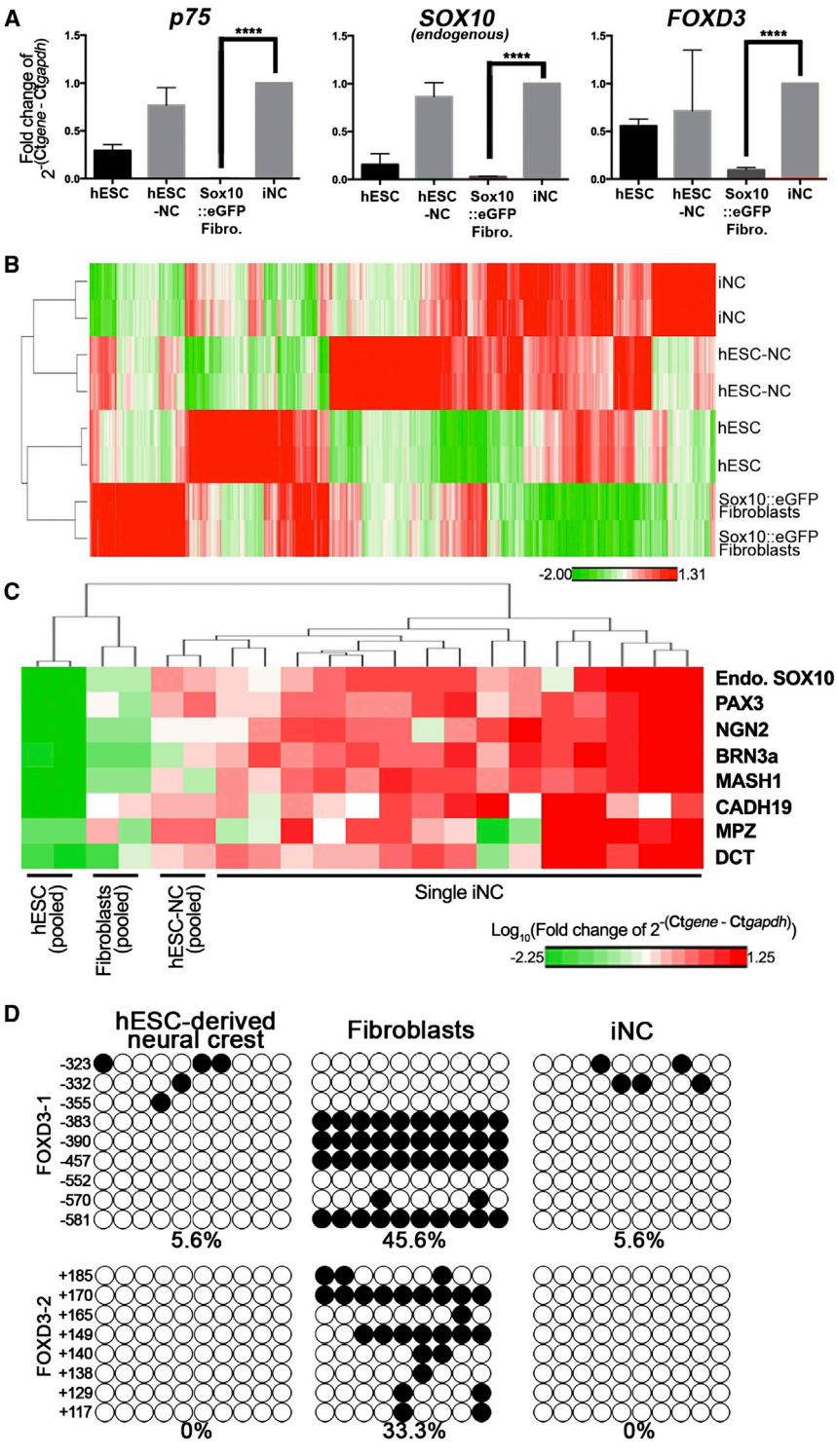

Figure 2. Detailed Molecular Profiling of iNCs Converted from *Sox10::eGFP* Fibroblasts

(A) Gene expression levels of *Sox10::eGFP*+ iNCs (*p75*, endogenous *SOX10* and *FOXD3*) are significantly higher than those of *Sox10::eGFP* fibroblasts (before iNC induction), but comparable to those of hESC-NCs. ****$p < 0.0001$.

(B) Clustered heat map of global gene expression.

(C) Single-cell gene expression analysis.

(D) Graphical representation of the methylation state using bisulphite-sequencing analysis of the *FOXD3* promoter. n = 3–4. All values are mean and SD. See also Figure S2.

OLIG2, *NKX2.2*, and *NKX6.2* were not detected (Figure S2B). Global gene expression in FACS-purified eGFP+ putative iNC and hESC-NC showed substantial downregulation of fibroblast-specific gene signatures and large-scale activation of genes specific to the NC lineage, resulting in a hierarchical clustering between hESC-NC- and eGFP-expressing iNCs over other cell types (Figure 2B). Based on our single-cell qRT-PCR analysis (Figures S2C–S2E), most of the FACS-purified single iNC cells showed robust expression of NC marker genes, similar to hESC-NC, and again exhibited hierarchical clustering between hESC-NC-expressing and all eGFP-expressing single iNC cells (Figure 2C). Comparison of the gene expression profiles between the hESC-NC and iNC populations identifies common upregulated genes, including known NC marker genes (including *TWIST1*, *SNAIL2*, *ITGA4*, *ITGA6*, *SOX5*, *SOX6*, *PLP1*, *Myelin Protein Zero* [*MPZ*], etc.). The differentially expressed genes between the hESC-NC and iNC populations fall into several categories—the upregulated gene list in iNC can be categorized according to melanocytic specification (melanocytic differentiation: $p = 0.02323$, pigment cell differentiation: $p = 0.02967$, pigment granule/melanosome: $p = 0.0006298$, pigmentation: $p = 0.02088$), whereas upregulated genes in hESC-NC are largely classified into two major categories, neuronal specification (neuron differentiation: $p = 8.52e^{-17}$, cell morphogenesis involved in neuron differentiation: $p = 2.40e^{-14}$, sensory organ development: $p = 1.73e^{-09}$) and NC migration (NC cell migration: $p = 0.03795$, migration: $p = 0.01590$). Furthermore, we monitored the DNA methylation status of two regions in *FOXD3* (Wahlbuhl et al., 2012), which showed drastic changes in the DNA methylation profile after iNC induction (Figure 2D). These data demonstrate that *Sox10::eGFP*-expressing iNCs obtain genetic and epigenetic similarity to hESC-NC, but not to fibroblasts or undifferentiated hESCs, in both a bulk and a single-cell manner.

To characterize cellular features as an NC, first we investigated the increased migration ability of *Sox10::eGFP*-expressing iNC over GFP(−) non-iNC populations (Figure S3A). To find their in vivo behaviors, freshly isolated iNC populations were grafted

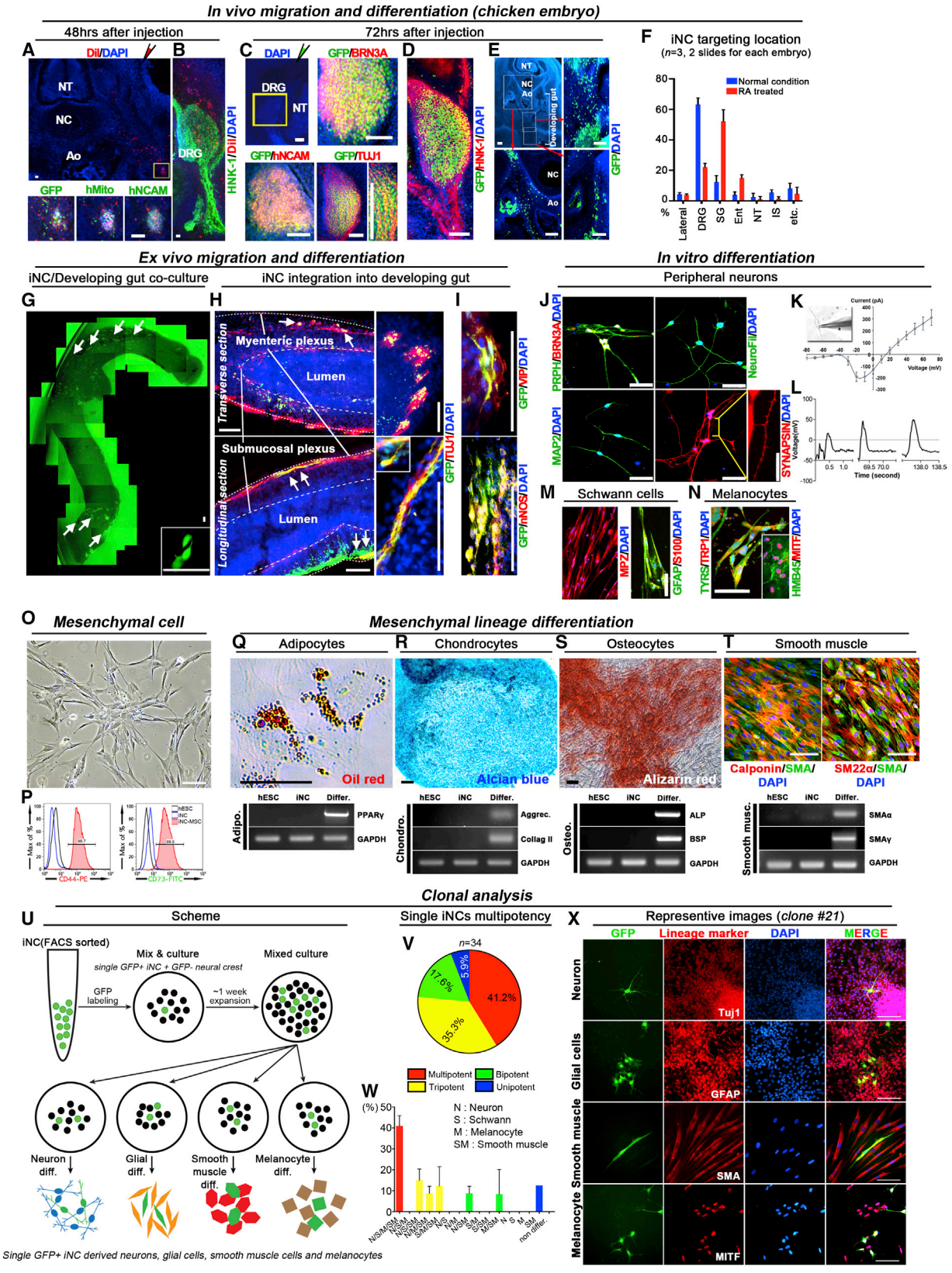

Single GFP+ iNC derived neurons, glial cells, smooth muscle cells and melanocytes

(legend on next page)

into the intersomite space of chick embryos (Lee et al., 2007) after being labeling with DiI dye (Figures 3A–3B and Figure S3C) or GFP (Figures 3C–3E, negative control shown in Figure S3B), and human cells were identified by either DiI dye or antibodies against GFP or human-specific markers (Figure 3A and Figure S3C). Two days after in ovo transplantation, we observed extensive migration of the iNC population throughout the embryo (Figures 3A and 3B). More importantly, 3 days after in ovo injection, we found much more efficient migration into the Dorsal Root Ganglia (DRG) region, where most of the GFP-labeled iNC population express BRN3A and TUJ1 (Figures 3C and 3D). As shown in Figures 3E–3F and Figure S3C, most of the transplanted iNC cells migrated into or resided in the expected regions, such as lateral part, DRG, Sympathetic Ganglia (SG), and enteric region. Because we found that the numbers of transplanted iNC cells migrating into ventral or gut region are relatively few (Figures 3E–3F and Figure S3C), we treated them with retinoic acid (RA) (Kawaguchi et al., 2010), but still there were small numbers of iNC that successfully migrated into developing gut (Figure 3F, total counted iNC number = 1,593). To find their enteric neuron commitment, we employed ex vivo coculture of iNC population with developing chicken guts. GFP+ iNC cells are populated near both ends of the gut and they have a typical ''locomotion-cell morphology'' (Figure 3G), suggesting that they are a presumably migrating population. We also found extensive numbers of GFP+ iNC cells in the myenteric plexus layer and near submucosal plexus layer with TUJ1 coexpression (Figure 3H), as well as neuronal nitric oxide synthase (nNOS) and vasoactive intestinal peptide (VIP) (Figure 3I) in the cryosection. In addition, we could find glial specification of cocultured GFP+ iNC, determined by GFAP staining (Figure S3D), but the percentage of GFAP+ cells are minimal (less than 1% among GFP+ iNC). Next, we assessed the in vitro differentiation potential of *Sox10::eGFP*+ iNCs upon withdrawal of SOX10 overexpression (Figure S3E). Neuronal differentiation was induced (Lee et al., 2010), and most of the surviving cells after neuronal differentiation are positive for TUJ1 (data not shown), BRN3A, Peripherin, Neurofilament, MAP2, Substance-P, Calcitonin Gene Related Peptide (CGRP), and Synapsin (Figure 3J and Figure S3F), which was confirmed again with qRT-PCR analysis for *NGN2* and *BRN3a* (Figure S3G). In particular, the I-V curve data (Figures 3K and 3L) demonstrate that Sox10::eGFP-fibroblast-iNC-derived neurons have a substantial amount of sodium channels and conduct current at a series of holding voltages in a manner comparable to that of rodent sensory neurons. Schwann cell differentiation from iNCs, as assessed by the expression of S100B, MPZ, and GFAP, was induced (Lee et al., 2010) (over 95% cells were GFAP+/S100B+) (Figure 3M) and corresponds to significant upregulation of Schwann cell lineage markers such as *DHH* and *GFAP* (Figure S3H). Likewise, isolated iNCs that differentiated into melanocytes (Mica et al., 2013) that express MITF, Premelanosome Protein, TRP1, and Tyrosinase (TYRS) (over 90% cells were positive) also showed a marked increase of melanocyte-specific marker expression, including *TYRS* and *MITF*, in comparison to *Sox10::eGFP* fibroblasts and freshly isolated iNCs (Figure 3N and Figure S3I). Most of the SOX10::eGFP+ iNC-derived mesenchymal cells (Lee et al., 2007) showed a typical morphology (Figure 3O) and express traditional mesenchymal cell surface markers (CD44 and CD73) (over 98%) (Figure 3P). Furthermore, we found that iNC-derived mesenchymal cells could differentiate into adipogenic, chondrogenic, osteogenic and smooth muscle cells as assessed by appropriate histocytochemistry/immunofluourescence and transcriptional analysis (Figures 3Q–3T).

To find their multipotency at a single-cell level, 34 clones of single iNC cells from hESC-derived fibroblasts were expanded, differentiated, and analyzed (two independent repeats; Figure 3U). After their differentiation toward the four lineages, we stained them with GFP antibody and each lineage marker (TUJ1 for neurons, GFAP for glia, SMA for smooth muscle cells, and MITF for melanocytes) and could address the differentiation potentials of clones of each iNC as shown in Figures 3V–3W. Surprisingly, we found that about 40% of single iNC clones from hESC-derived fibroblasts could give rise to four different

Figure 3. Differentiation Potential of iNCs Converted from *Sox10::eGFP* Reporter Fibroblasts

(A–E) Representative images of in ovo transplanted iNCs labeled with DiI dye (red, A and B) or GFP labeling (green, C–E) with viral transduction after iNC isolation. Arrows in the top of (A) (red) and (C) (green) show the injection site. The yellow boxes in the left panels (A and C) mark the area enlarged in other panels. Migrated (for 48 hr) DiI+ iNC population (A) was double-confirmed with GFP, human-mitochondria-specific antibody (hMito), and human-specific NCAM antibody (hNCAM) (A). Migratory stream of injected iNC population (red, DiI) is overlapped with endogenous host (chicken) NC (HNK1, green) (B). After 72 hr after injection, a GFP-labeled iNC population expressing BRN3a, hNCAM, and TUJ1 (C), costained with HNK1 antibody (D), was located in DRG. A GFP-labeled iNC population migrated into the developing gut region (E). NT, neural tube; NC, notochord; Ao, aorta; DRG, dorsal root ganglion.

(F) Comparison of iNC migration/targeting region after in ovo transplantation with or without retinoic acid (RA) treatment. Ent, enteric region; IS, injection site.

(G–I) Representative images of ex vivo coculture of embryonic developing gut with FACS-purified iNCs. After 4 days of coculture, GFP-labeled iNCs were observed (G, large image), and magnified morphology of iNC was shown (in right bottom of G). (H and I) iNCs (green) were colabeled with TUJ1 (red), shown in transverse and longitudinal sections (H), and enlarged images show expression of VIP and nNOS in GFP+ iNC neurons (I).

(J) Representative images of differentiated iNCs stained with peripheral neuron markers.

(K and L) Functional characterization of iNC-derived neurons, including current-voltage curve (I-V curve, K) and the action potentials, upon high levels of KCl administration (L).

(M and N) Differentiation of iNC into Schwann cells (M) and melanocytes (N) with marker expression.

(O–T) iNCs were differentiated into mesenchymal lineages. Representative images of mesenchymal cellular morphology (O), and FACS plot with mesenchymal marker (CD44 and CD73) (P), are shown. Sublineage differentiation into adipocytes (Q, upper), chondrocytes (R, upper), osteocytes (S, upper) and smooth muscle cells (T, upper) was confirmed with histocytochemistry or antibody staining, followed by specific marker gene expression for each lineage (lower panels in each image).

(U–X) Clonal analysis with single iNC cells, illustrated in (U). (V–X) Proportion of the multipotency level among iNC clones (V and W), based on coexpression of GFP and each lineage marker (X). Representative images are for neurons, glia, smooth muscle cells, and melanocytes, respectively.

Scale bars correspond to 50 μm for (A), (B), and (J–N) (except for Synapsin, which indicates 10 μm); 500 μm for (C) and (D); and 100 μm for (E), (G), (H), (I), and (O–X). See also Figure S3.

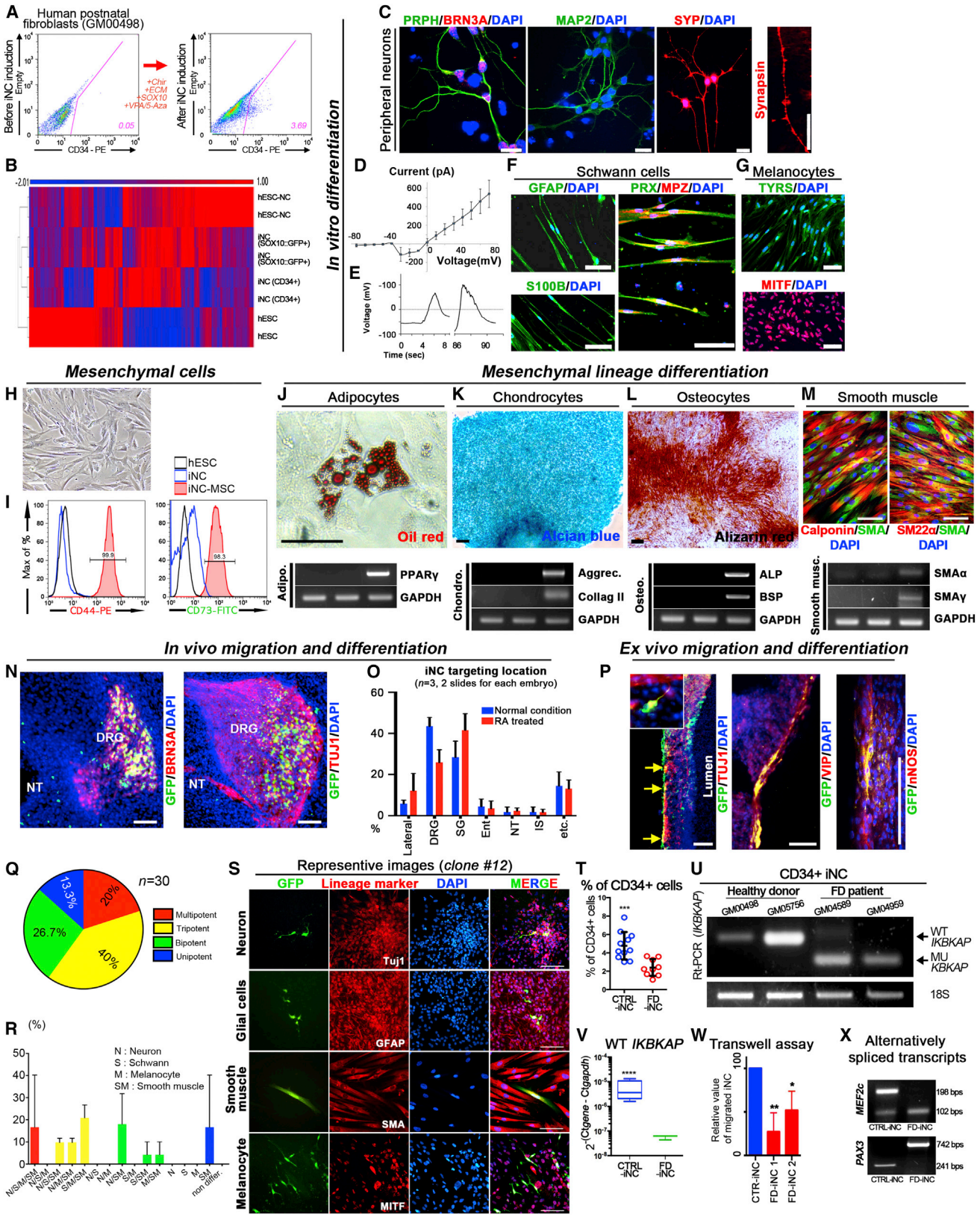

(legend on next page)

lineages (Figures 3W–3X) (“quadpotent”), whereas about 35% of single iNC clones from hESC-derived fibroblasts are competent to become three lineages (tripotent). This result is comparable to our previous hESC-NC study (Lee et al., 2007), in which an average of 65% of FACS-purified p75+/HNK1+ single cells differentiated into triple lineages (neurons, glia, and smooth muscle cells). Taken together, these experiments show the in vivo and in vitro evidences for migration ability and multilineage differentiation potential (even at the clonal level) of isolated SOX10::eGFP+ iNCs.

Because p75 is already expressed in postnatal fibroblasts (Figures S4A–S4D), we profiled the known NC cell surface marker expression in postnatal fibroblasts before and after iNC induction, and we found that one CD marker (CD34) is not expressed before iNC induction but is present at the final stage of iNC induction (Figures S4C and S4D). We also confirmed the absence of *SOX10* expression in each postnatal fibroblast by single-cell qRT-PCR while they expressed *Collagen* (Figure S4E). NC cells and their progeny express CD34 in different postnatal tissues (Chen et al., 2012; Yoshida et al., 2006), and this marker is also expressed in iNC population derived from Sox10::eGFP fibroblasts (Figure S4F). Although CD34 is also known for expression in the hematopoietic lineages, we could not find any evident hematopoietic marker gene expression (Figure S4G). Comparable efficiency of CD34+ cells after iNC induction of postnatal fibroblasts (GM00498, 3.32% ± 0.16%; GM05756, 4.99% ± 1.47%) was achieved (Figure 4A and Figure S4H). A higher level of NC marker gene expression was detected in CD34+ iNCs as opposed to the level in postnatal fibroblasts (before induction) (Figure S4I, upper panel). Detailed transcriptional comparison (Figure 4B) with differentially expressed genes and hierarchical analysis shows that hESC-fibroblast-derived iNC (Sox10::eGFP+ population; e-iNC) and postnatal-fibroblast-derived iNC (CD34+ population; p-iNC) are clustered to each other, rather than to hESC-NC population or undifferentiated hESCs. The list of commonly and significantly upregulated genes between e-iNC (Sox10::eGFP+ population) and p-iNC (CD34+ population) includes early NC marker genes (*PAX3*, *ZIC1*, *FOXD3*, *TLX*, *MSX2*, and *TWIST*), sensory neuron marker genes (*NEUROG1*, *NEUROD1*, *POU4F1*, and *ISL1*), Schwann cell marker genes (*MPZ*), melanocyte marker genes (*DCT* and *TYRP1*), etc. (Figure S4J). Interestingly, comparison of gene ontology analysis with both e-iNC (SOX10::eGFP+) and p-iNC (CD34+) shows that pigment granule ($p = 3.22e^{-04}$) related and melanosome ($p = 3.22e_{-04}$) related genes are upregulated in CD34+ p-iNC. Furthermore, we differentiated CD34+ p-iNC into peripheral neurons and Schwann cells. Even though 20% of cells were dead during neuronal differentiation, 85% of survived cells were TUJ1+ cells (data not shown). As shown in Figure 4C, p-iNC-derived neurons express BRN3a, Peripherin, MAP2, Synaptophysin, and Synapsin. The electrophysiological recordings revealed that those p-iNC derived neurons are functional (Figures 4D and 4E), exhibiting action potentials with current injection and high levels of potassium treatment. For Schwann cell differentiation, sorted p-iNC was subject to the culture condition, same as in Figure S3E. Three weeks after culture, we could find strong immunoreactivity of Schwann cells markers, GFAP, periaxin (PRX), MPZ, and S100B, in most of the cells (90%) (Figure 4F). Melanocytes were also achieved and confirmed by antibody staining with the specific markers MITF and TYRS, and 95% of cells were positive after 7 days of differentiation (Figure 4G). Furthermore, we differentiated p-iNC into mesenchymal lineages, resulting in typical cellular morphology (Figure 4H) and expression of traditional mesenchymal cell surface markers (CD44 and CD73) (Figure 4I). We also found that p-iNC-derived mesenchymal cells could give rise into adipogenic, chondrogenic, osteogenic, and smooth muscle cells (Figures 4J–4M).

After injection of GFP-labeled p-iNC into the intersomite region of chick embryos, most of the cells had migrated and were targeted to DRG (Figure 4N) and SG, and few cells were targeted into the developing gut region (Figure 4O, total counted iNC number = 551). Because of small numbers of cells that localized

Figure 4. Direct Conversion of Human Normal and Patient Postnatal Fibroblasts into iNCs

(A) Representative FACS plot of CD34 antibody staining before and after iNC induction of human postnatal fibroblasts (GM00498).

(B) Clustered heat map of global gene expression of four samples including iNC derived from postnatal fibroblasts, iNC derived from *Sox10::eGFP* fibroblasts (iNC), hESC-NC, and undifferentiated hESCs (hESC).

(C) Differentiation of postnatal iNC into neuron markers.

(D and E) Functional characterization of postnatal iNC-derived neurons, including the current-voltage curve (I-V curve, D) and the action potentials, upon high levels of KCl administration (E).

(F) Differentiation of iNC into Schwann cells with expression of GFAP, S100B, Periaxin (PRX), and MPZ.

(G) Differentiation potentials of postnatal iNC into melanocyte lineage, stained with TYRS and MITF antibodies.

(H and I) Postnatal CD34+ iNC could differentiate into mesenchymal cells with typical morphology (H) and surface marker expression (CD44 and CD73) (I).

(J–M) Sublineage differentiation into adipocytes (J), chondrocytes (K), osteocytes (L), and smooth muscle cells (M).

(N) GFP-labeled postnatal iNC was located in DRG with expression of BRN3a and TUJ1.

(O) Migration/targeting regions of postnatal iNC with or without RA treatment.

(P) Representative images of ex vivo coculture of embryonic developing gut with postnatal CD34+ iNC with expression of putative enteric neuron markers (TUJ1, VIP, and nNOS).

(Q–S) Percentage of the different multipotency levels among individual postnatal iNC clones (Q and R), based on GFP and lineage marker coexpression (S). Representative images are shown for neurons, glia, smooth muscle cells, and melanocytes, respectively.

(T) Decreases in the percentage levels of CD34 in FD fibroblasts as compared to that of control fibroblasts.

(U) Wild-type (WT) *IKBKAP* transcript was found in CD34+ iNCs from healthy donor fibroblasts. In contrast, in CD34+ iNCs from FD patient fibroblasts, WT *IKBKAP* was not detected, but mutant (MU) *IKBKAP* was expressed. Additional qRT-PCR data show a significant difference in WT *IKBKAP* expression between the two populations (V).

(W) A transwell assay shows the defective migration ability of FD-iNC.

(X) Alternatively spliced transcripts of *MEF2C* and *PAX3*. The size of the PCR product is shown in the right side of each gel image. n = 3–7.

All values are mean and SD. *$p < 0.05$; **$p < 0.01$; ***$p < 0.0005$; ****$p < 0.0001$. Scale bars correspond to 50 μm for panels (C)–(G) (except for Synapsin, which indicates 10 μm) and 10 μm for (H)–(S). See also Figure S4.

in the enteric region, we performed ex vivo coculture of gut with GFP-labeled p-iNC to confirm their ability to differentiate and migrate into the enteric nervous system. After coculture, GFP-labeled p-iNC cells were distributed around both myenteric and submucosal plexuses, as confirmed by immunostaining with TUJ1, VIP, and nNOS (Figure 4P). To find the multipotency of individual p-iNC cells, we performed single-cell analysis as shown in Figure 3U. A total of 30 clones of single CD34+ iNC cells from postnatal fibroblasts were analyzed (two independent repeats). Upon staining with GFP and lineage marker antibodies (Figures 4Q and 4R), we learned that 20% of single iNC clones from postnatal fibroblasts could become four different lineages (multipotent or quadpotent) (Figure 4S), whereas 40% of single iNC clones from postnatal fibroblasts are competent to become three lineages (tripotent), which is comparable to that of SOX10::eGFP+ iNC (Figures 3V–3X).

To evaluate whether iNCs from familial dysautonomia (FD) patient fibroblasts show characteristics similar to those in our previous hiPSC-based study (Lee et al., 2009), we isolated CD34+ cells after iNC induction from two different FD fibroblasts (GM04959 and GM04589) (Figures S4K–S4I). Although the percentage of CD34+ cells in FD patient fibroblasts (2.403% ± 0.3051%, n = 9) (at Day 14 of iNC induction) was a significantly ($p = 0.0006$) lower than that of healthy donor fibroblasts (4.769% ± 0.4494%, n = 11) (Figure 4T), we found remarkable enrichment of NC marker gene expression (Figure S4I, lower panel). To examine the transcriptional similarity of CD34+ iNCs at the single-cell level, we profiled gene expression levels of NC markers using our single-cell quantitative RT-PCR with each FACS-purified CD34+ iNC (Figure S4M). Most of the single cells in the FACS-purified CD34+ iNCs population showed robust expression of NC marker genes. These data suggest that CD34 can enrich the iNC populations derived from postnatal fibroblasts, and that isolated CD34+ iNCs obtain an NC gene expression and transcriptional profile similar to those of hESC-NC, but not similar to those of postnatal human fibroblasts or undifferentiated hESCs.

A single point mutation in the IKBKAP (also known as ELP1, a subunit of Elongator complex) gene lowers the level of wild-type *IKBKAP* expression, as shown in postmortem FD patient samples (Slaugenhaupt et al., 2001) and our hiPSC-based study (Lee et al., 2009). In our current study, we confirmed that CD34+ iNCs converted from FD fibroblasts show significantly decreased levels of wild-type *IKBKAP* expression, as shown in the representative gel image of *IKBKAP* splicing levels ascertained via RT-PCR and qRT-PCR ($p < 0.0001$) (Figures 4U and 4V). Furthermore, to investigate potential disease mechanisms underlying FD, we performed a comparative transcriptome analysis with FACS-purified CD34+ FD-iNCs (two genotypes) versus control-iNCs (CTRL-iNCs) (two genotypes), and expression levels of key transcripts from the microarray study were confirmed by qPCR analysis (Figure S4L). Intriguingly, we found that the expression levels of 412 transcripts (among 36,000 probe sets) are decreased in FD-iNCs versus control-iNCs (fold-change $\geq$2-fold; corrected $p = 0.05$), and about one-third of the downregulated genes (36.2%) in FD-hiPSC-derived NC (Lee et al., 2009) are also found in the list of downregulated genes of FD-iNCs. Importantly, gene ontology analysis (using the DAVID web-based program for functional annotation analysis; http://david.abcc.ncifcrf.gov) revealed that commonly downregulated genes (191 transcripts) in both the current FD-iNC study and our previous FD-hiPSC-based study (Lee et al., 2009) were significantly linked to alternative splicing ($p = 0.0002094$, 98 transcripts, 52.12%) and cell migration ($p = 0.0000586$, 17 transcripts, 9.04%). The FD-specific cell migration defect was represented in our previous FD-hiPSC study as well as other studies (Close et al., 2006), but the involvement of alternative splicing (except for the IKBKAP gene) has not been discussed in FD studies. First, to confirm a disease-related migration phenotypes, a transwell assay was performed with freshly purified CD34+ FD-iNCs (two different genotypes; FD-iNC 1: GM04959 and FD-iNC 2: GM02341) that showed significantly decreased migratory ability over that of CD34+ control iNC (GM05756), as shown in Figure 4W and Figure S4N. To further examine splicing aberrations, we designated primer sets for RT-PCR of two different genes, *MEF2C* (Hakim et al., 2010) and *PAX3* (Parker et al., 2004), and we found alternatively spliced forms in FD-iNCs (in both GM04959 and GM02341) (Figure 4X), while the expression levels of the housekeeping gene (*GAPDH*) were comparable (data not shown) between CTRL-iNCs and FD-iNCs. In *MEF2C* transcripts of FD-iNC, the gamma region between exon 9 and exon 10 is skipped, though it was included in CTRL-iNC (Figure S4O). For the *PAX3* transcripts a different type of isoform D was found in FD-iNC (Figure S4O). All the PCR products are verified by sequencing (data not shown), suggesting a potential role for an altered splicing in FD pathogenesis. Importantly, we found that FD-specific hiPSC-derived NC population also exhibits splicing aberrations in *PAX3* and *MEF2C* similar to those of FD-iNC (Figure S4P). These data show that our aberrant splicing events in *PAX3* and *MEF2c* transcripts are indeed a unique feature in the NC cell type, demonstrating the feasibility of direct conversion of human postnatal fibroblasts into iNC populations.

DISCUSSION

Here we show that NC identity can be directly acquired from human fibroblasts by the delivery of a single transcription factor (SOX10) and cell-extrinsic cues (Figures 1A–1D and Figures S1K–S1M), as determined by morphological (Figures 1F–1G and Figure S1Q), molecular (Figure 1G, Figure 2, and Figures S2A and S2B), and cellular (Figure 3 and Figure S3) analysis. Furthermore, by using a cell surface marker (CD34), we could prospectively isolate the iNC populations directly converted from human postnatal fibroblasts (Figure 4A and Figure S4I). As a proof of principal, patient-specific iNCs were achieved from FD patient fibroblasts (Figures S4I–S4K), exhibiting disease-relevant characteristics, such as decreased level of direct conversion efficiency, transcriptional misregulation (*IKBKAP* and other transcripts), defective migration ability (Lee et al., 2009), and previously unknown altered splicing events (Figures 4T–4X and Figures S4L–S4P).

Although SOX10 is a transcription factor related to NC and oligodendrocyte development, we could not detect any gene expression of oligodendrocyte markers (Figure S2B). This finding can be explained by the important role of cell extrinsic cues (e.g., the WNT pathway in NC formation) (García-Castro et al., 2002), such as the critical function of Chir99021 during iNC induction

(Figures 1D and 1G). In contrast, additional BMP activation hampers the direct conversion process toward iNC fate (Figure S1U). Our current study demonstrates that environmental cues along with cell intrinsic factors could play important roles in iNC fate determination, which should be applicable to other direct conversion studies.

Disease-specific iNC provides an opportunity for understanding previously unknown disease mechanisms of NC disorders such as FD. First, we found that FD fibroblasts have reduced efficiency on iNC direct conversion, which might be explained by other group's study that *IKBKAP* protein and other subunits of Elongator complex are involved in the demethylation process (Okada et al., 2010). Our current study demonstrates that FD-iNC showed decreased migration ability (Figure 4W and Figure S4N) and alternative splicing (Figure 4X and Figure S4O) in transcripts of *MEF2C* (Hakim et al., 2010) and *PAX3* (Parker et al., 2004). The expression levels of these genes are closely linked to NC lineages (Wang et al., 2006), Waardenburg syndrome (Pingault et al., 2010), and a neuromuscular disorder (Bachinski et al., 2010). Abnormal splicing events might be related to the role of *IKBKAP* protein, which binds to unspliced pre-mRNA (Gilbert et al., 2004), and it is plausible to hypothesize that the impaired Elongator-RNA interaction directly or indirectly compromises the general splicing machinery, which remains to be proven. Going forward, it would be intriguing to compare the results of the our hiPSC and current iNC studies with those of NC derived from preimplantation genetic diagnosis (PGD) embryo-derived hESC lines with the *IKBKAP* mutation.

Collectively, by employing a single genetic factor and multiple environmental cues, postnatal fibroblasts of both healthy donors and patients can be directly converted into a functional and multipotent iNC cell population that exhibits disease-relevant phenotypes.

EXPERIMENTAL PROCEDURES

Detailed procedures can be found in the Supplemental Experimental Procedures.

Fibroblasts

Sox10::eGFP BAC-transformed hESCs were differentiated into fibroblasts using 10% serum containing MEM (Invitrogen) and maintained for 12 weeks. The postnatal fibroblasts from healthy donors (GM00498 and GM05756) and FD patients (GM04589 and GM04959) were purchased from Coriell.

iNC Induction

To induce iNC populations, 1 × 10^5 cells/well were plated in 12-well tissue culture plates after FN/Lam or indicated cellular matrix coating. After 24 hr, cells were treated with 1 uM of 5-Aza (Sigma), 1 mM of VPA (Stemgent), or TrichostatinA (Sigma) in 1 μg/ml DOX (Sigma) containing Neurobasal medium for 24 hr. Then, fresh Neurobasal medium containing 1 μg/ml of DOX was added with 3 uM of Chir99021 (Tocris). At Day 14 of induction, FACS analysis or FACS sorting was performed.

Ex Vivo Gut/iNC Coculture

Developing chicken guts were taken from chick embryos (H&H Stage 35–38) and cocultured with GFP-labeled iNCs in Neurobasal medium on the low attachment surface plate for 24 hr. Then, embryonic guts were vigorously washed with PBS and cultured with Neurobasal medium containing 20 ng/ml of BDNF, 20 ng/ml of GDNF, and 200 nM of ascorbic acid for 10–14 days. Cryosectioned guts were stained following the IHC protocol. For RA treatment, we used 1 uM RA for FACS-purified iNC (for 24 hr) before coculture.

SUPPLEMENTAL INFORMATION

Supplemental Information for this article includes four figures, Supplemental Experimental Procedures, and one table and can be found with this article online at http://dx.doi.org/10.1016/j.stem.2014.07.013.

ACKNOWLEDGMENTS

We would like to thank the Lee lab members for valuable discussions. G.L. is a New York Stem Cell Foundation (NYSCF) Robertson Investigator and this research was supported by NYSCF and the Maryland Stem Cell Research Fund (TEDCO). We thank Dr. Mica, Dr. Cheng, Ms. Mukherjee-Clavin, and Dr. Fossati for sharing cDNA.

Received: June 21, 2013
Revised: June 19, 2014
Accepted: July 29, 2014
Published: August 21, 2014

REFERENCES

Bachinski, L.L., Sirito, M., Böhme, M., Baggerly, K.A., Udd, B., and Krahe, R. (2010). Altered MEF2 isoforms in myotonic dystrophy and other neuromuscular disorders. Muscle Nerve *42*, 856–863.

Betancur, P., Bronner-Fraser, M., and Sauka-Spengler, T. (2010). Assembling neural crest regulatory circuits into a gene regulatory network. Annu. Rev. Cell Dev. Biol. *26*, 581–603.

Chen, X., Thomson, H., Hossain, P., and Lotery, A. (2012). Characterisation of mouse limbal neurosphere cells: a potential cell source of functional neurons. Br. J. Ophthalmol. *96*, 1431–1437.

Close, P., Hawkes, N., Cornez, I., Creppe, C., Lambert, C.A., Rogister, B., Siebenlist, U., Merville, M.P., Slaugenhaupt, S.A., Bours, V., et al. (2006). Transcription impairment and cell migration defects in elongator-depleted cells: implication for familial dysautonomia. Mol. Cell *22*, 521–531.

García-Castro, M.I., Marcelle, C., and Bronner-Fraser, M. (2002). Ectodermal Wnt function as a neural crest inducer. Science *297*, 848–851.

Gilbert, C., Kristjuhan, A., Winkler, G.S., and Svejstrup, J.Q. (2004). Elongator interactions with nascent mRNA revealed by RNA immunoprecipitation. Mol. Cell *14*, 457–464.

Hakim, N.H., Kounishi, T., Alam, A.H., Tsukahara, T., and Suzuki, H. (2010). Alternative splicing of Mef2c promoted by Fox-1 during neural differentiation in P19 cells. Genes Cells *15*, 255–257.

Kawaguchi, J., Nichols, J., Gierl, M.S., Faial, T., and Smith, A. (2010). Isolation and propagation of enteric neural crest progenitor cells from mouse embryonic stem cells and embryos. Development *137*, 693–704.

Kelsh, R.N. (2006). Sorting out Sox10 functions in neural crest development. Bioessays *28*, 788–798.

Lee, G., Kim, H., Elkabetz, Y., Al Shamy, G., Panagiotakos, G., Barberi, T., Tabar, V., and Studer, L. (2007). Isolation and directed differentiation of neural crest stem cells derived from human embryonic stem cells. Nat. Biotechnol. *25*, 1468–1475.

Lee, G., Papapetrou, E.P., Kim, H., Chambers, S.M., Tomishima, M.J., Fasano, C.A., Ganat, Y.M., Menon, J., Shimizu, F., Viale, A., et al. (2009). Modelling pathogenesis and treatment of familial dysautonomia using patient-specific iPSCs. Nature *461*, 402–406.

Lee, G., Chambers, S.M., Tomishima, M.J., and Studer, L. (2010). Derivation of neural crest cells from human pluripotent stem cells. Nat. Protoc. *5*, 688–701.

Mica, Y., Lee, G., Chambers, S.M., Tomishima, M.J., and Studer, L. (2013). Modeling neural crest induction, melanocyte specification, and disease-related pigmentation defects in hESCs and patient-specific iPSCs. Cell Rep *3*, 1140–1152.

Okada, Y., Yamagata, K., Hong, K., Wakayama, T., and Zhang, Y. (2010). A role for the elongator complex in zygotic paternal genome demethylation. Nature *463*, 554–558.

Pang, Z.P., Yang, N., Vierbuchen, T., Ostermeier, A., Fuentes, D.R., Yang, T.Q., Citri, A., Sebastiano, V., Marro, S., Südhof, T.C., and Wernig, M. (2011). Induction of human neuronal cells by defined transcription factors. Nature *476*, 220–223.

Park, I.H., Arora, N., Huo, H., Maherali, N., Ahfeldt, T., Shimamura, A., Lensch, M.W., Cowan, C., Hochedlinger, K., and Daley, G.Q. (2008). Disease-specific induced pluripotent stem cells. Cell *134*, 877–886.

Parker, C.J., Shawcross, S.G., Li, H., Wang, Q.Y., Herrington, C.S., Kumar, S., MacKie, R.M., Prime, W., Rennie, I.G., Sisley, K., and Kumar, P. (2004). Expression of PAX 3 alternatively spliced transcripts and identification of two new isoforms in human tumors of neural crest origin. Int. J. Cancer *108*, 314–320.

Pingault, V., Ente, D., Dastot-Le Moal, F., Goossens, M., Marlin, S., and Bondurand, N. (2010). Review and update of mutations causing Waardenburg syndrome. Hum. Mutat. *31*, 391–406.

Schäfer, B.W., Blakely, B.T., Darlington, G.J., and Blau, H.M. (1990). Effect of cell history on response to helix-loop-helix family of myogenic regulators. Nature *344*, 454–458.

Sekiya, S., and Suzuki, A. (2011). Direct conversion of mouse fibroblasts to hepatocyte-like cells by defined factors. Nature *475*, 390–393.

Sieber-Blum, M. (2000). Factors controlling lineage specification in the neural crest. Int. Rev. Cytol. *197*, 1–33.

Sieber-Blum, M., and Zhang, J.M. (1997). Growth factor action in neural crest cell diversification. J. Anat. *191*, 493–499.

Slaugenhaupt, S.A., Blumenfeld, A., Gill, S.P., Leyne, M., Mull, J., Cuajungco, M.P., Liebert, C.B., Chadwick, B., Idelson, M., Reznik, L., et al. (2001). Tissue-specific expression of a splicing mutation in the IKBKAP gene causes familial dysautonomia. Am. J. Hum. Genet. *68*, 598–605.

Son, E.Y., Ichida, J.K., Wainger, B.J., Toma, J.S., Rafuse, V.F., Woolf, C.J., and Eggan, K. (2011). Conversion of mouse and human fibroblasts into functional spinal motor neurons. Cell Stem Cell *9*, 205–218.

Takahashi, K., and Yamanaka, S. (2006). Induction of pluripotent stem cells from mouse embryonic and adult fibroblast cultures by defined factors. Cell *126*, 663–676.

Vierbuchen, T., Ostermeier, A., Pang, Z.P., Kokubu, Y., Südhof, T.C., and Wernig, M. (2010). Direct conversion of fibroblasts to functional neurons by defined factors. Nature *463*, 1035–1041.

Wahlbuhl, M., Reiprich, S., Vogl, M.R., Bösl, M.R., and Wegner, M. (2012). Transcription factor Sox10 orchestrates activity of a neural crest-specific enhancer in the vicinity of its gene. Nucleic Acids Res. *40*, 88–101.

Wang, Q., Kumar, S., Slevin, M., and Kumar, P. (2006). Functional analysis of alternative isoforms of the transcription factor PAX3 in melanocytes in vitro. Cancer Res. *66*, 8574–8580.

Yoshida, S., Shimmura, S., Nagoshi, N., Fukuda, K., Matsuzaki, Y., Okano, H., and Tsubota, K. (2006). Isolation of multipotent neural crest-derived stem cells from the adult mouse cornea. Stem Cells *24*, 2714–2722.